PROPER SGS HEAT FLUX MODELS AND NUMERICAL METHODS FOR LES

F.X. Trias[1], *D. Santos*[1], *F. Dabbagh*[2], *A. Gorobets*[3], *A. Oliva*[1]

[1] *Heat and Mass Transfer Technological Center, Technical University of Catalonia, C/Colom 11, 08222 Terrassa (Barcelona)*
[2] *Christian Doppler Laboratory for Multi-Scale Modeling of Multiphase Processes, Johannes Kepler University, Altenbergerstraße 69, 4040 Linz, Austria.*
[3] *Keldysh Institute of Applied Mathematics, 4A, Miusskaya Sq., Moscow 125047, Russia.*

francesc.xavier.trias@upc.edu

Abstract

In this work, we aim to shed light to the following research question: *can we find a nonlinear tensorial subgrid-scale (SGS) heat flux model with good physical and numerical properties, such that we can obtain satisfactory predictions for buoyancy-driven turbulent flows?* This is motivated by our findings showing that the classical (linear) eddy-diffusivity assumption fails to provide a reasonable approximation for the actual SGS heat flux: namely, *a priori* analysis for air-filled Rayleigh-Bénard convection (RBC) clearly shows a strong misalignment. In the quest for more accurate models, we firstly study and confirm the suitability of the eddy-viscosity assumption for RBC carrying out *a posteriori* tests for different models at very low Prandtl numbers (liquid sodium, Pr=0.005) where no heat flux SGS activity is expected. Then, a new tensorial SGS heat flux model is proposed and studied *a priori* using DNS data of an air-filled (Pr=0.7) RBC at Rayleigh numbers up to 10^{11}. Apart from having good alignment trends with the actual SGS heat flux, it is numerically stable *per se* and has the proper cubic near-wall behavior. Our near future research plans include testing *a posteriori* this new tensorial SGS heat flux model. Prior to that, we also aim to properly discretize these models in space and time.

1 Introduction

In the last decades, many engineering/scientific applications have benefited from the advances in the field of Computational Fluid Dynamics (CFD). Unfortunately, most of practical turbulent flows cannot be directly computed from the Navier-Stokes (NS) equations because not enough resolution is available to resolve all the relevant scales of motion. Therefore, practical numerical simulations have to resort to turbulence modeling. We may therefore turn to large-eddy simulation (LES) to predict the large-scale behavior of turbulent flows. In LES, the large scales of motions are explicitly computed, whereas effects of small scale motions are modeled. Since the advent of CFD, many subgrid-scale models have been proposed and successfully applied to a wide range of flows. Eddy-viscosity models for LES is probably the most popular example thereof. Then, for problems with the presence of active/passive scalars (*e.g.* heat transfer problems, transport of species in combustion, dispersion of contaminants,...) the (linear) eddy-diffusivity assumption is usually chosen. However, this type of approximation systematically fails to provide a reasonable approximation of the actual SGS flux because they are strongly misaligned (see Higgins et al. (2004); Chumakov (2008)). This was clearly shown in our previous works Dabbagh et al. (2017, 2020) where SGS features were studied *a priori* for a RBC at Ra-number up to 10^{11} (see Figure 1). This leads to the conclusion that nonlinear (or tensorial) models are necessary to provide good approximations of the actual SGS heat flux. In this regard, the nonlinear Leonard model by Leonard (1997), which is the leading term of the Taylor series of the SGS heat flux, provides a very accurate *a priori* approximation. However, the local dissipation introduced by the model can take negative values; therefore, the Leonard model cannot be used as a standalone SGS heat flux model, since it produces a finite-time blow-up. A similar problem is encountered with the nonlinear tensorial model proposed by Peng & Davidson (2002). An attempt to overcome these instability issues is the so-called mixed model (see Higgins et al. (2004)), where the Leonard model is combined with an eddy-diffusivity model.

2 On a proper tensorial SGS heat flux model

In this context, we planned to shed light to the following research question: *can we find a nonlinear subgrid-scale heat flux model with good physical and numerical properties, such that we can obtain satisfactory predictions for buoyancy-driven turbulent flows?* To that end, we consider nonlinear SGS heat flux models that can adequately represent the dynamics of the smallest (unresolved) scales, overcom-

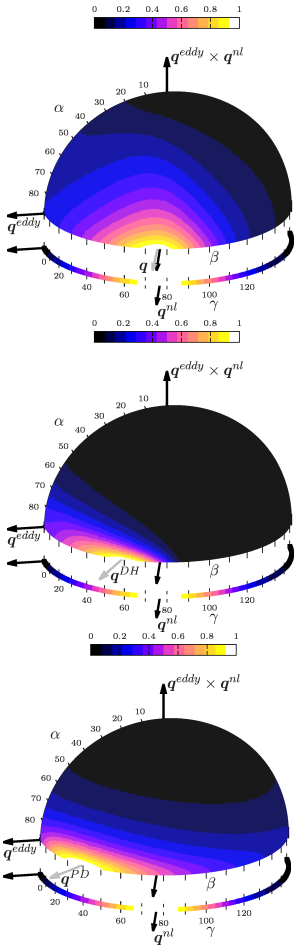

Figure 1: Joint probability distribution functions (JPDF) of the angles (α, β) plotted on a half unit sphere to show the orientation in the space of the mixed model. From top to bottom, alignment trends of the actual SGS heat flux, $\boldsymbol{q}$, the Daly & Harlow (1970) model, $\boldsymbol{q}^{DH}$, and the Peng & Davidson (2002) model, $\boldsymbol{q}^{PD}$. For simplicity, the JPDF and the PDF magnitudes are normalized by its maximal. For details the reader is referred to Dabbagh et al. (2017).

ing the above-mentioned inherent limitations of the eddy-diffusivity models Dabbagh et al. (2017, 2020). The specific SGS models that we consider consist of a linear eddy-viscosity term for momentum supplemented by a nonlinear model for the SGS heat flux. Firstly, we have studied and confirmed the suitability of the eddy-viscosity assumption for buoyancy-driven turbulent flows. To do so, a set of simulations at $Pr = 0.005$ (liquid sodium) have been carried out at $Ra = 7.14 \times 10^6$ and $Ra = 7.14 \times 10^7$. Figure 2 displays a snapshot of the temperature and velocity magnitude for the DNS simulation at the highest Ra. This clearly illustrates the separation between the smallest scales of temperature and velocity, *i.e.* the ratio between the Kolmogorov length scale and the Obukhov-Corrsin length scale is given by $Pr^{3/4}$ (see Sagaut (2005)). Therefore, for a $Pr = 0.005$ (liquid sodium) we have a separation of more than one decade. Hence, it is possible to combine an LES simulation for the velocity field with the numerical resolution of all the relevant scales of the thermal field. Regarding this, results shown in Figure 3 seem to confirm the adequacy of eddy-viscosity models for this kind of flows. Namely, Figure 3 shows the Nusselt number for a set of meshes and eddy-viscosity models: the WALE model by Nicoud & Ducros (1999), the Vreman (2004) model, the QR model by Verstappen (2011) and the S3QR model proposed by Trias et al. (2015). Results obtained without SGS model are also shown to illustrate the effect of the eddy-viscosity models to improve the solution. At first sight it can be observed that, in general, all LES solutions are in rather good agreement with the DNS data even for the coarsest grids ($48 \times 26 \times 26$ for $Ra = 7.14 \times 10^6$ and $96 \times 52 \times 52$ for $Ra = 7.14 \times 10^7$ whereas only the finest ones ($128 \times 72 \times 72$ and $192 \times 104 \times 104$ at $Ra = 7.14 \times 10^6$ and $512 \times 288 \times 288$ at $Ra = 7.14 \times 10^7$) can provide accurate results when the model is switched off. A closer inspection shows that slightly better results are obtained for those eddy-viscosity models (WALE and S3QR) that have the proper near-wall behavior, *i.e.* $\nu_e = \mathcal{O}(y^3)$. To emphasize the benefits of LES modeling, the approximate computational cost of the simulations is displayed in the top horizontal axis of Figure 2 (top and middle): it was measured on the MareNostrum 4 supercomputer and corresponds to a total integration period of 500 time-units. Finally, to see the effect of eddy-viscosity models in more detail, results for the average turbulent kinetic energy are shown in Figure 2 (bottom) for two meshes and two eddy-viscosity models (WALE and S3QR). All these results seem to confirm the suitability of the eddy-viscosity assumption for buoyancy-driven flows. For more details the reader is referred to Trias et al. (2020).

Then, in the quest for more accurate models, we recently proposed a new family of tensorial SGS heat flux models (see Trias et al. (2020), for details). Among all possible candidates, we have chosen the so-called S2PR model given by

$$\boldsymbol{q}^{S2PR} = -C_{s2pr} P_{\mathsf{G}\mathsf{G}^T}^{-3/2} R_{\mathsf{G}\mathsf{G}^T}^{1/3} \frac{\delta^2}{12} \mathsf{G}\mathsf{G}^T \nabla \overline{T}, \qquad (1)$$

with $C_{s2pr} \approx 12.02$, where $P_{\mathsf{G}\mathsf{G}^T}$ and $R_{\mathsf{G}\mathsf{G}^T}$ are the first and third invariants of the $\mathsf{G}\mathsf{G}^T$ tensor, respectively. This tensor is proportional to the gradient model by Clark et al. (1979) given by the leading term of the Taylor series expansion of the subgrid stress tensor $\tau(\overline{\boldsymbol{u}}) = (\delta^2/12)\mathsf{G}\mathsf{G}^T + \mathcal{O}(\delta^4)$. This model shows a very good representation of the SGS heat flux both in direction and magnitude (see Figure 4). Moreover, apart from fulfilling a set of desirable properties (locality, Galilean invariance, numerical stability, proper near-wall behavior, and automatically switch-off for laminar and 2D flows), the proposed model is well-conditioned, and has a low computational cost and no

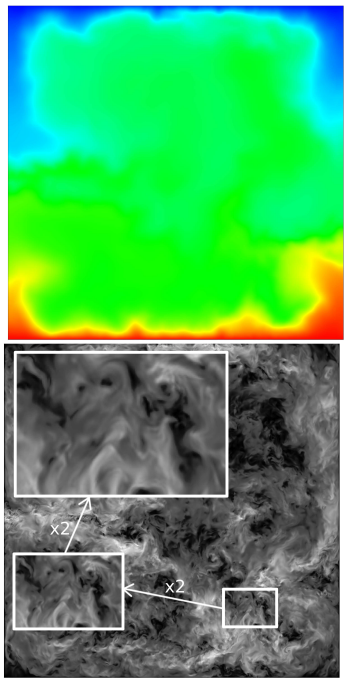

Figure 2: An instantaneous picture of the temperature field (top) and velocity magnitude (bottom), $|\boldsymbol{u}|$, of the DNS simulation of RBC at $Ra = 7.14 \times 10^7$ and $Pr = 0.005$ (liquid sodium) carried out using a mesh of $966 \times 966 \times 2048 \approx 1911M$ grid points. See the movie in the database (http://www.cttc.upc.edu/downloads/RBC_lowPr).

intrinsic limitations for statistically in-homogeneous flows. Hence, it seems to be well suited for engineering applications. Our near future research plans include the extension of this analysis to higher Ra and testing *a posteriori* the new non-linear SGS heat flux models for air-filled RBC at Ra up to 10^{11}. Prior to that, we aim to properly discretize tensorial eddy-diffusivity models. A first approximation to this problem is presented below.

3 On the proper discretization of a tensorial eddy-diffusivity model

Spatial discretization

Let us firstly consider the spatial discretization of a tensorial eddy-diffusivity model, *i.e.*

$$\nabla \cdot \boldsymbol{q} \approx \nabla \cdot \left(\mathsf{A}\nabla\overline{T}\right). \tag{2}$$

Notice that all the tensorial models referred in this work, including the one presented in Eq.(1), fall in this template. We aim to preserve fundamental physical and mathematical properties when discretizing Eq.(2) where A is a 3×3 real-valued tensor (2×2 for 2D flows). Namely, the first property denoted as **Property P1** is the conservation of the integral of $\overline{T}$,

$$\int_\Omega \nabla \cdot (\mathsf{A}\nabla\overline{T}) dV = \int_{\partial\Omega} (\mathsf{A}\nabla\overline{T}) \cdot \boldsymbol{n} dS = 0, \tag{3}$$

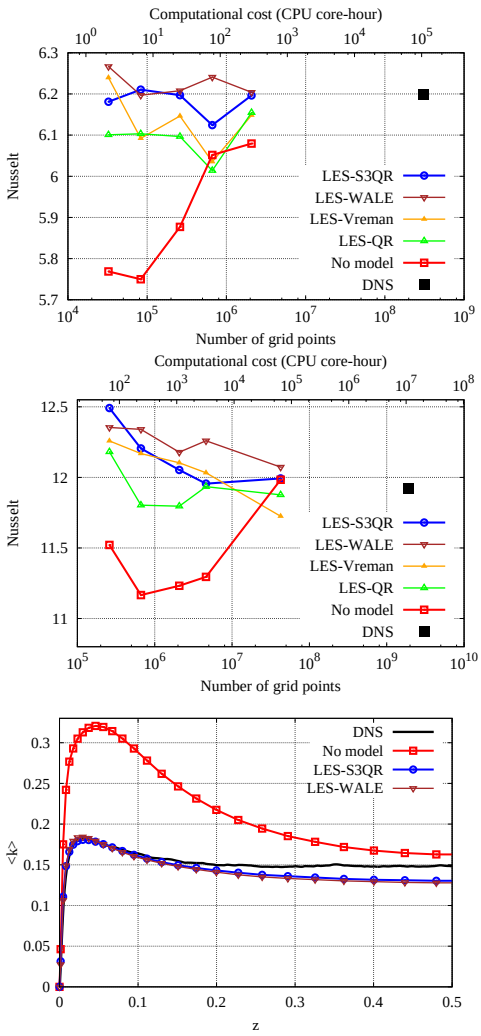

Figure 3: Comparison of LES (and no-model) versus DNS results of liquid sodium ($Pr = 0.005$) RBC. Average Nusselt for different meshes at $Ra = 7.14 \times 10^6$ (top) and $Ra = 7.14 \times 10^7$ (middle). Computational costs at the MareNostrum 4 supercomputer are shown in the top of the plots. Bottom: LES results at $Ra = 7.14 \times 10^6$ of turbulent kinetic energy at the cavity mid-width for a $96 \times 52 \times 52$ mesh compared with the DNS results obtained on a mesh of $488 \times 488 \times 1280 \approx 305M$.

assuming that contribution from boundary, $\partial\Omega$, vanishes. The second property [**Property P2**] is the symmetry preservation: Eq.(2) represents a diffusive operator (no interscale interaction). Hence, $\nabla \cdot \mathsf{A}\nabla$ is a symmetric operator if the tensor A is symmetric,

$$\begin{aligned} < \psi, \nabla \cdot (\mathsf{A}\nabla\theta) > &= - < \nabla\psi, \mathsf{A}\nabla\theta > \\ &\overset{\mathsf{A}=\mathsf{A}^T}{=} - < \mathsf{A}\nabla\psi, \nabla\theta > \\ &= < \nabla \cdot (\mathsf{A}\nabla\psi), \theta >, \end{aligned} \tag{4}$$

where $< a, b >= \int_\Omega abdV$ is the usual inner-product of functions. Notice that the gradient is the adjoint of minus the divergence operator (and vice versa) provided that contributions from boundary, $\partial\Omega$, cancel, *i.e.* $\int_\Omega \nabla \cdot (\boldsymbol{a}b)dV =< \boldsymbol{a}, \nabla b > + < \nabla \cdot \boldsymbol{a}, b >=$

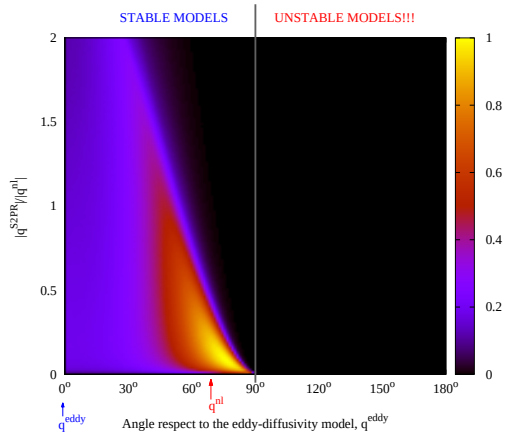

Figure 4: Joint PDF for the S2PR model (Eq. 1) in the space $(|\boldsymbol{q}^{S2PR}|/|\boldsymbol{q}^{nl}|, \beta)$ where the angle β is defined in Figure 1. The analyzed data corresponds to the bulk region of the air-filled RBC configuration at $Ra = 10^{11}$ studied in Dabbagh et al. (2020).

$\int_{\partial\Omega} \boldsymbol{a}b \cdot \boldsymbol{n} dS = 0$. The third property [**Property P3**] is the definiteness preservation; that is, given a positive (or negative) definite tensor, A, then the operator $\nabla \cdot \mathsf{A}\nabla$ is negative (or positive) semi-definite,

$$< \nabla \cdot (\mathsf{A}\nabla\theta), \theta > = - < \mathsf{A}\nabla\theta, \nabla\theta > \overset{\mathsf{A}=\mathsf{L}\mathsf{L}^T}{=} - < \mathsf{L}\nabla\theta, \mathsf{L}\nabla\theta >= -||\mathsf{L}\nabla\theta||^2 \leq 0, \quad (5)$$

where the Cholesky decomposition of the tensor A, $\mathsf{A} = \mathsf{L}\mathsf{L}^T$, assumes that A is a symmetric positive definite tensor. For negative definite tensors, $\mathsf{A} = -\mathsf{L}\mathsf{L}^T$, leading to the conclusion that $\nabla \cdot \mathsf{A}\nabla$ is then positive semi-definite. Two more properties of numerical nature can be added to the list. Namely, [**Property P4**] states that it is preferable to build up discretizations that are entirely based on already existing discrete operators in a standard CFD code. This obviously facilitates the implementation, the portability and the verification of the method. Finally, it is also desirable to naturally recover the numerical result obtained for an isotropic diffusive term, *i.e.* $\mathsf{A} = \kappa\mathsf{I}$. This last property will be referred as [**Property P5**].

First property **P1** relies on the Gauss theorem. Thus, Eq.(2) is discretized in divergence form,

$$\mathsf{M}\boldsymbol{q}_s \in \mathbb{R}^n, \quad (6)$$

where $\mathsf{M} \in \mathbb{R}^{n\times m}$ represents the divergence operator in integral form, n and m are respectively the number of control volumes and faces on the computational domain, and $\boldsymbol{q}_s \in \mathbb{R}^m$ is a discrete vector that contains the (turbulent) heat fluxes defined at the faces of the volumes. The subindices c and s refer to whether the variables are cell-centered or staggered at the faces. Otherwise stated, we follow the same notation used in Trias et al. (2014). Then, everything relies on the computation of $\boldsymbol{q}_s$; therefore, hereafter we assume that

$$\boldsymbol{q}_s = \boldsymbol{q}_s(\mathsf{A}_c, \boldsymbol{T}_c) \in \mathbb{R}^m, \quad (7)$$

where A_c is the cell-centered discrete counterpart of tensor A and $\boldsymbol{T}_c$ is the cell-centered discrete temperature field. Furthermore, we can assume that the following discrete operators are already available: the discrete gradient operator, $\mathsf{G} \in \mathbb{R}^{m\times n}$, diagonal matrices containing the staggered, $\Omega_s \in \mathbb{R}^{m\times m}$, and cell-centered, $\Omega_c \in \mathbb{R}^{n\times n}$, control volumes and a cell-to-face interpolator, $\Pi_{c\to s} \in \mathbb{R}^{m\times n}$. To simplify the analysis we consider a 2D Cartesian mesh (extension to 3D is straightforward).

Heat fluxes, $\boldsymbol{q}_s$, can be approximated as follows

$$\boldsymbol{q}_s^{\mathbf{D1}} = \tilde{\mathsf{A}}_s^{\mathbf{D1}}\mathsf{G}T \text{ where } \tilde{\mathsf{A}}_s^{\mathbf{D1}} = \tilde{\Pi}_{c\to s}\tilde{\mathsf{A}}_c\tilde{\Pi}_{s\to c}, \quad (8)$$

where $\tilde{\Pi}_{c\to s}$ and $\tilde{\mathsf{A}}_c$ are block matrices given by

$$\tilde{\Pi}_{c\to s} = \begin{pmatrix} \Pi_{c\to x} & 0 \\ 0 & \Pi_{c\to y} \end{pmatrix} \quad \tilde{\mathsf{A}}_c = \begin{pmatrix} \mathsf{A}_c^{xx} & \mathsf{A}_c^{xy} \\ \mathsf{A}_c^{xy} & \mathsf{A}_c^{yy} \end{pmatrix}. \quad (9)$$

where $\mathsf{A}_c^{xx} \in \mathbb{R}^{n\times n}$, $\mathsf{A}_c^{xy} \in \mathbb{R}^{n\times n}$ and $\mathsf{A}_c^{yy} \in \mathbb{R}^{n\times n}$ are diagonal matrices containing the cell-centered components of the symmetric tensor A. Then, to preserve the symmetry (**P2**) and the definiteness (**P3**) properties, the above-mentioned duality between the gradient and the divergence operators

$$\mathsf{G} = -\Omega_s^{-1}\mathsf{M}^T, \quad (10)$$

must be preserved together with the following relationship between interpolators

$$\tilde{\Pi}_{s\to c} \equiv \Omega^{-1}\tilde{\Pi}_{c\to s}^T\Omega_s, \quad (11)$$

where $\Omega = \mathsf{I}_2 \otimes \Omega_c$ (for 2D) and $\Omega = \mathsf{I}_3 \otimes \Omega_c$ (for 3D) where $\mathsf{I}_2 \in \mathbb{R}^{2\times 2}$ and $\mathsf{I}_3 \in \mathbb{R}^{3\times 3}$ are identity matrices. Hereafter, this discretization method is referred as **Method D1**. By construction, this method satisfies all the properties (**P1-P4**) except **P5**, *i.e.* due to the additional interpolations, $\tilde{\Pi}_{c\to s}$ and $\tilde{\Pi}_{s\to c}$, it does not recover the numerical solution obtained for isotropic diffusivity, *i.e.* $\mathsf{A} = \kappa\mathsf{I}$. This forces to redefine Eq.(8) and the subsequent definitions. Namely,

$$\boldsymbol{q}_s^{\mathbf{D2}} = \tilde{\mathsf{A}}_s^{\mathbf{D2}}\mathsf{G}T \text{ where} \quad (12)$$
$$\tilde{\mathsf{A}}_s^{\mathbf{D2}} = \tilde{\Pi}_{c\to s}\tilde{\mathsf{A}}_c^{off}\tilde{\Pi}_{s\to c} + \mathrm{diag}(\tilde{\Pi}_{c\to s}\,\mathrm{diag}(\tilde{\mathsf{A}}_c)),$$

where $\tilde{\mathsf{A}}_c^{off}$ represents the off-diagonal elements of $\tilde{\mathsf{A}}_c$ given in Eq.(9). Hence, the only difference between methods **D2** and **D1** is the treatment of the diagonal terms. In this way, we avoid unnecessary interpolations for the coefficients of the diagonal matrices A_c^{xx} and A_c^{yy}. Moreover, we preserve the same discretization for the isotropic case; therefore, all properties (**P1-P5**) are preserved. This second method is referred as **Method D2**.

Temporal discretization

Explicit (or semi-explicit) time-integration schemes impose severe restrictions on the time-step, Δt, due to the fact that the eigenvalues of the amplification matrix must lie inside the stability region of the

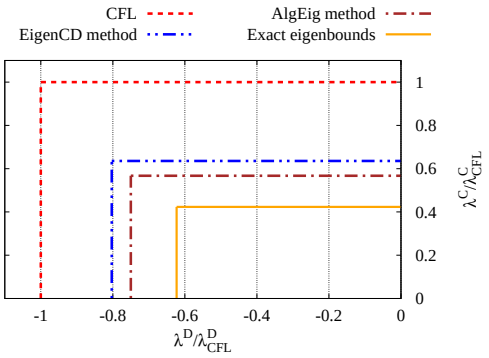

Figure 5: Comparison between different approaches to compute bounds for the eigenvalues of the convective and diffusive operators given in Eqs.(17) and (18). Results correspond to a set of 100 randomly generated incompressible velocity fields and diffusivity constants for a uniformly spaced Cartesian mesh. Eigenbounds are normalized for the results obtained using the classical CFL condition given in Eqs.(15) and (16). Other approaches correspond to the *EigenCD* approach proposed in Trias & O. Lehmkuhl (2011) and the *AlgEig* approach proposed here in Eqs.(19) and (20).

scheme. In the particular case of the NS equations, or in general for any convection-diffusion equation, these eigenvalues are directly related with the eigenvalues of the convective, $\mathsf{C}(\boldsymbol{u}_s)$, and diffusive, D, discrete operators. The simplest example to show this, is a convection-diffusion equation without source terms discretized (in time) using a first-order explicit Euler scheme:

$$\Omega_c \frac{\boldsymbol{\phi}_c^{n+1} - \boldsymbol{\phi}_c^n}{\Delta t} + \mathsf{C}(\boldsymbol{u}_s)\,\boldsymbol{\phi}_c^n = \mathsf{D}\boldsymbol{\phi}_c^n, \tag{13}$$

which can be easily re-arranged as follows

$$\boldsymbol{\phi}_c^{n+1} = (\mathsf{I} + \Delta t \mathsf{R}(\boldsymbol{u}_s))\,\boldsymbol{\phi}_c^n, \tag{14}$$

where $\mathsf{R}(\boldsymbol{u}_s) \equiv \Omega_c^{-1}(-\mathsf{C}(\boldsymbol{u}_s) + \mathsf{D})$. Hence, the stability of the time-integration scheme is guaranteed if the spectral radius of the amplification matrix is smaller than one, *i.e.* $\rho(\mathsf{I} + \Delta t \mathsf{R}(\boldsymbol{u}_s)) \leq 1$. This imposes restrictions on the eigenvalues of the matrix $\Delta t \mathsf{R}(\boldsymbol{u}_s)$ which obviously depend on the eigenvalues of the convective and diffusive operators and the value of Δt. Hence, the proper bounding of the eigenvalues of $\mathsf{C}(\boldsymbol{u}_s)$ and D is a cornerstone for the performance of CFD codes. In this regard, most of them rely on the well-known CFL condition which provides bounds for the eigenvalues of the convective and diffusive terms,

$$\lambda^{\mathsf{C}}_{\text{CFL}} = \frac{1}{C_C} \max_k \left\{ \sum_{i=1}^{3} \frac{|U_i|}{\Delta x_i} \right\}, \tag{15}$$

$$\lambda^{\mathsf{D}}_{\text{CFL}} = \frac{1}{C_D} \max_k \left\{ \frac{\nu}{\Delta x_k^2} \right\}. \tag{16}$$

However, this type of conditions may become inaccurate especially for highly skewed meshes where CFL-based criteria tend to overpredict the eigenvalues of the dynamical system (see Figure 5). This effect becomes even more relevant for unstructured formulations. This was analyzed in detail in Trias & O. Lehmkuhl (2011) where a self-adaptive strategy was proposed. Firstly, the eigenvalues of the dynamical system were bounded by means of an inexpensive method named *EigenCD* which basically relies on the application of the Gershgorin circle theorem to provide more accurate bounds of the matrices $\mathsf{C}(\boldsymbol{u}_s)$ and D. Nevertheless, the application of this method on an algebraic framework is not straightforward unless a new specific kernel is implemented. This would go against the philosophy followed in Álvarez et al. (2021): minimizing the number of basic computational kernels is crucial to facilitate portability across the variety and complexity of incoming computational architectures in the current HPC exascale race. In this context, we propose a new method that only relies on basic algebraic kernels such as the sparse matrix-vector product (SpMV). Shortly, the convective and diffusive matrices can be expressed in term of even more basic operators,

$$\mathsf{C}(\boldsymbol{u}_s) = \mathsf{M}\mathsf{U}_s\Pi_{c\to s} = \frac{1}{2}\mathsf{T}_{sc}\mathsf{A}_s\mathsf{U}_s|\mathsf{T}_{cs}|, \tag{17}$$

$$\mathsf{D} = \mathsf{M}\Lambda\mathsf{G} = -\mathsf{T}_{sc}\mathsf{A}_s\Lambda_s\Delta_s^{-1}\mathsf{T}_{cs}, \tag{18}$$

where A_s, U_s, Λ_s and Δ_s are diagonal matrices containing the corresponding face areas, velocities, diffusivities and distances between adjacent nodes. Moreover, T_{sc} and $\mathsf{T}_{cs} = \mathsf{T}_{sc}^T$ are the face-to-cell and the cell-to-face incidence matrices, respectively. Recalling that a square matrix and its transpose have the same spectrum, we can easily show that given two rectangular matrices, $\mathsf{A} \in \mathbb{R}^{n\times m}$ and $\mathsf{B} \in \mathbb{R}^{m\times n}$, both square matrices $\mathsf{AB} \in \mathbb{R}^{n\times n}$ and $\mathsf{A}^T\mathsf{B}^T \in \mathbb{R}^{m\times m}$ have the same non-zero eigenvalues. At this point, we can use this property to explore matrices whose eigenvalues are the same as $\mathsf{C}(\boldsymbol{u}_s)$ and D defined in Eqs.(17) and (18). Among all the option tested the optimal ones are:

$$\lambda^{\mathsf{C}}_{\text{AlgEig}} = \frac{1}{2}\max\left(\tilde{\boldsymbol{f}}_{\boldsymbol{s}}^{\,1/2} \circ |\mathsf{T}_{cs}\Omega_c^{-1}|\mathsf{T}_{cs}^T||\tilde{\boldsymbol{f}}_{\boldsymbol{s}}^{\,1/2}\right), \tag{19}$$

$$\lambda^{\mathsf{D}}_{\text{AlgEig}} = \max\left(|\mathsf{T}_{cs}\Omega_c^{-1}\mathsf{T}_{cs}^T|\,\text{diag}(\tilde{\Lambda}_s)\right), \tag{20}$$

where $\tilde{\boldsymbol{f}}_{\boldsymbol{s}} = \text{diag}(\mathsf{A}_s\mathsf{U}_s)$, $\tilde{\Lambda}_s = \mathsf{A}_s\Lambda_s\Delta_s^{-1}$ and $\circ$ represents the Hadamard product. Figure 5 displays a comparison between the new approach named *AlgEig*, the *EigenCD* method proposed in Trias & O. Lehmkuhl (2011) and the classical CFL approach. Although computationally unaffordable for practical problems, the exact computation of the eigenbounds is also shown for comparison. It is remarkable that apart from its inherent portability, this new approach also provides better results than existing approaches.

4 Concluding remarks

Nowadays, most of the CFD codes rely on the eddy-diffusivity assumption, $\boldsymbol{q}^{eddy} \propto \nabla\overline{T}$, to model the SGS heat flux for LES simulations. Researchers' experience carrying out LES simulations of buoyancy-driven turbulence using this approach is, in general, quite frustrating. Namely, in many cases there is no relevant improvement compared with the results obtained without any SGS model. In other cases, the apparent improvement is simply due to the fact that the SGS model stabilizes the numerical simulation that otherwise (without model) would just blow up. The latter issue can be solved using numerical discretizations that are stable *per se* Trias et al. (2014). In any case, very small improvements are actually observed Dabbagh et al. (2017) leading to the necessity to use very fine grids (sometimes similar to DNS) to obtain reliable solutions. Furthermore, *a priori* analysis using DNS data of RBC at high Ra-numbers clearly shows that the classical (linear) eddy-diffusivity assumption is completely misaligned with the actual SGS heat flux Dabbagh et al. (2017, 2020). In this regard, our near future research plans include testing *a posteriori* the new tensorial SGS heat flux model given in Eq.(1) for air-filled RBC problems at Ra up to 10^{11}. Prior to that, we also aim to properly discretize these models both in space and time. As mentioned above, the underlying spatial discretization can play a crucial role in the performance of SGS models. Regarding the temporal discretization a new accurate and portable approach for bounding the eigenvalues of the convective and diffusive operators has been proposed. Results will be presented during the conference.

Acknowledgments

F.X.T., F.D. and A.O. have been supported by the *Ministerio de Economía y Competitividad*, Spain, ANUMESOL project (ENE2017-88697-R). F.X.T. and A.O. are supported by the Generalitat de Catalunya RIS3CAT-FEDER, FusionCAT project (001-P-001722) and by the Clean Sky 2 Joint Undertaking, ANTIFOD project (grant ID 821352). F.D. is supported by the Austrian Federal Ministry for Digital and Economic Affairs, the National Foundation for Research, Technology and Development, and the K1MET center for metallurgical research in Austria (www.k1-met.com). D.S. is supported by an FI AGAUR-Generalitat de Catalunya grant (2020FI B 00839). Calculations were performed on the MareNostrum 4 supercomputer at the BSC. The authors thankfully acknowledge these institutions.

References

Álvarez, X., Gorobets, A., & Trias, F. X. (2021). A hierarchical parallel implementation for heterogeneous computing. Application to algebra-based CFD simulations on hybrid supercomputers. *Computers & Fluids*, *214*, 104768.

Chumakov, S. G. (2008). "*A priori* study of subgrid-scale flux of a passive scalar in isotropic homogeneous turbulence. *Physical Review E*, *78*, 036313.

Clark, R. A., Ferziger, J. H., & Reynolds, W. C. (1979). Evaluation of subgrid-scale models using an accurately simulated turbulent flow. *Journal Fluid Mechanics*, *91*, 1–16.

Dabbagh, F., Trias, F. X., Gorobets, A., & Oliva, A. (2017). A priori study of subgrid-scale features in turbulent Rayleigh-Bénard convection. *Physics of Fluids*, *29*, 105103.

Dabbagh, F., Trias, F. X., Gorobets, A., & Oliva, A. (2020). Flow topology dynamics in a three-dimensional phase space for turbulent Rayleigh-Bénard convection. *Physical Review Fluids*, *5*, 024603.

Daly, B. J., & Harlow, F. H. (1970). Transport equations in turbulence. *Physics of Fluids*, *13*, 2634.

Higgins, C. W., Parlange, M. B., & Meneveau, C. (2004). The heat flux and the temperature gradient in the lower atmosphere. *Geophysical Research Letter*, *31*, L22105.

Leonard, A. (1997). Large-eddy simulation of chaotic convection and beyond. *AIAA paper*, *97-0304*.

Nicoud, F., & Ducros, F. (1999). Subgrid-scale stress modelling based on the square of the velocity gradient tensor. *Flow, Turbulence and Combustion*, *62*(3), 183–200.

Peng, S., & Davidson, L. (2002). On a subgrid-scale heat flux model for large eddy simulation of turbulent thermal flow. *International Journal of Heat and Mass Transfer*, *45*, 1393–1405.

Sagaut, P. (2005). *Large Eddy Simulation for Incompressible Flows: An Introduction*. Springer, 3^{rd} ed.

Trias, F. X., Dabbagh, F., Gorobets, A., & Oliet, C. (2020). On a proper tensor-diffusivity model for large-eddy simulation of buoyancy-driven turbulence. *Flow, Turbulence and Combustion*, *105*, 393–414.

Trias, F. X., Folch, D., Gorobets, A., & Oliva, A. (2015). Building proper invariants for eddy-viscosity subgrid-scale models. *Physics of Fluids*, *27*(6), 065103.

Trias, F. X., & O. Lehmkuhl (2011). A self-adaptive strategy for the time-integration of Navier-Stokes equations. *Numerical Heat Transfer, part B*, *60*(2), 116–134.

Trias, F. X., O. Lehmkuhl, A. Oliva, C.D. Pérez-Segarra, & R.W.C.P. Verstappen (2014). Symmetry-preserving discretization of Navier-Stokes equations on collocated unstructured meshes. *Journal of Computational Physics*, *258*, 246–267.

Verstappen, R. (2011). When does eddy viscosity damp subfilter scales sufficiently? *Journal of Scientific Computing*, *49*(1), 94–110.

Vreman, A. W. (2004). An eddy-viscosity subgrid-scale model for turbulent shear flow: Algebraic theory and applications. *Physics of Fluids*, *16*(10), 3670–3681.